Journal of Aerosol Science 126 (2018) 33–46

Contents lists available at ScienceDirect

Journal of Aerosol Science

journal homepage: www.elsevier.com/locate/jaerosci

Mechanical stability measurements of surface modified nanoparticle agglomerates

P. Post[1], M. Bierwirth[1,*], A.P. Weber

Institute of Particle Technology, Clausthal University of Technology, Leibnizstr. 19, 38678 Clausthal-Zellerfeld, Germany

ARTICLE INFO

Keywords:
Fragmentation
Low pressure impaction
Mechanical stability
Nanoparticles
Particle coating
Plasma assisted chemical vapor deposition

ABSTRACT

A low pressure impactor is used to measure the mechanical stability of nanoparticle agglomerates. The stability at different impaction velocities is quantified as changes in the projection area of agglomerate fragments deposited on TEM grids mounted on the impaction plate. Platinum particles produced in a spark discharge generator are used as model particles. The mechanical stability of unmodified Pt-agglomerates is compared with the ones of thermally pretreated and coated agglomerates. The coatings are produced in a plasma assisted chemical vapor deposition process using the post-discharge environment of a dielectric barrier discharge. The coating process allows the coating of particles with silica at ambient temperature and so minimizes structural changes of the agglomerates before impaction. The precursors utilized are tetraethyl orthosilicate for silica and hexamethyldisiloxane for silica-organic coatings. Both coatings improve the stability of the agglomerates as indicated by reduced structural changes during impaction. The silica-organic coating, which is applied at 200 °C, seems to prevent sinter-related changes to the particles, which is observed for the uncoated particles at this temperature. This is further corroborated by the deposition behavior of these coated particles, which resembles more that of the original particles at 24 °C. Furthermore, the rebound behavior of coated agglomerates impacting on the TEM grid is shown. It is found that a minority of the particles rebound back from the TEM grid into the gas, which occurs in parallel to the structural changes.

1. Introduction

The mechanical stability of agglomerates is determined by the adhesion forces acting at the contact areas between individual primary particles. Particles can adhere to each other due to solid contacts, such as sintering necks, capillary forces of adsorbed liquids, electrostatic forces and van-der-Waals forces. If counteracting external forces exceed the adhesion forces, the agglomerate may restructure or fragment. Such external forces can include thermal (Weber & Friedlander, 1997), ultrasonic (Kusters, Pratsinis, Thoma, & Smith, 1993), electrostatic (Svestka, Cermak, & Grün, 1993) or shear forces (Eggersdorfer, Kadau, Herrmann, & Pratsinis, 2010). The resulting deagglomeration is of interest when smaller particles are desired, e.g. in medical (Voss & Finlay, 2002) or food (Guraya & James, 2002) applications. However, many other applications rely on stable bonds between primary particles, e.g. particulate coatings on substrates (Stepien et al., 2013).

The mechanical stability of nanoparticle agglomerates in the gas-phase was extensively studied in impactors. Due to the small mass of nanoparticles, high velocities are required to impact them onto a surface with sufficient energy to overcome the adhesion

* Corresponding author.
E-mail address: malte.bierwirth@tu-clausthal.de (M. Bierwirth).
[1] The authors contributed equally to the paper.

https://doi.org/10.1016/j.jaerosci.2018.08.007
Received 4 May 2018; Received in revised form 14 August 2018; Accepted 19 August 2018
Available online 22 August 2018
0021-8502/

forces. This can be achieved in a low pressure impactor (LPI), where the impaction is accomplished at pressures of a few mbar. Froeschke, Kohler, Weber, and Kasper (2003) demonstrated this method for the study of the fragmentation behavior of different particle materials. Seipenbusch, Toneva, Peukert, and Weber (2007) used such a setup to compare the binding strength of different metal agglomerates bound by van-der-Waals and magnetic forces. The influence of the degree of sintering on the stability of silica agglomerates was studied by Seipenbusch et al. (2010), who found a clear correlation between a reduction in fragmentation and the sintering temperature. Gensch and Weber studied the influence of the impaction angle and the rebound behavior of particles (Gensch & Weber, 2014, 2017). Ihalainen et al. studied the simultaneous breakup and bounce of different materials in a micro-orifice uniform deposit impactor (Ihalainen, Lind, Torvela, Lehtinen, & Jokiniemi, 2012). They found that the bounced fraction of the particles and the deposited fraction resulted in similar size distributions. Furthermore, they found that the degree of fragmentation depends on the primary particle size with agglomerates of smaller particles being harder to fragment (Froeschke et al., 2003; Ihalainen, Lind, Arffman, Torvela, & Jokiniemi, 2014). Since the degree of fragmentation depends on the particle material as well as the cross-sectional area of contact between primary particles, a coating of a more rigid material on the agglomerate should improve its stability during impaction.

There are multiple methods for coating nanoparticles with different shell materials, many of which use liquid-phase processes. However, while these liquid-phase methods may lead to homogeneous and defined coatings, they often require many process steps to extract the powder in the desired purity, such as removal of by-products, washing, and filtering. In contrast, gas-phase processes generally involve fewer steps and can be more easily coupled with subsequent powder modification or measurement methods. Common gas phase coating techniques include the flame synthesis (Qi, Moiseev, Deubener, & Weber, 2011; Teleki, Heine, Krumeich, Akhtar, & Pratsinis, 2008) or the atomic layer deposition (George, 2010). However, both often expose the powder to elevated temperatures during the process, which can lead to restructuring or sintering of the particles. Hence, if thermally unstable particles need to be coated, alternative coating techniques are preferable. Some plasma assisted processes provide a chemically reactive environment without the necessity of high temperatures. Furthermore, they allow the continuous coating of particles directly in the gas-phase and are for the most part independent of the particle synthesis method. The dielectric barrier discharge (DBD) is a relatively simple way to produce a non-thermal plasma and can be used for the coating of particles with different materials. Examples include the work of Vons, Creyghton, and Schmidt-Ott (2006), Nessim, Boulos, and Kogelschatz (2009), Marino, Huijser, Creyghton, and van der Heijden (2007) and Lei, Tang, Li, Luo, and Zhang (2007). The coating of particles is often accomplished directly in the plasma discharge. However, due to the strong electric fields this can result in the deposition of particles or coating material on the reactor walls, which decreases the long-term stability of the process. In the present work, a post-discharge plasma process was used (Post, Jidenko, Weber, & Borra, 2016; Post, Wurlitzer, Maus-Friedrichs, & Weber, 2018; Post & Weber, 2018). Here, neither the particles nor the precursors pass the discharge volume. Instead, the post-discharge environment of a DBD reactor is used to provide the reactive species necessary for the chemical vapor deposition (CVD) coating reactions. The precursors used here were tetraethyl orthosilicate (TEOS) and hexamethyldisiloxane (HMDSO), both of which are common for silica coatings. In this post-plasma process, the use of TEOS results in inorganic SiO_x coatings on the particles, while HMDSO-based coatings are silica-organic in nature (Post, Wurlitzer, et al., 2018). Two different variations of the post-plasma process were used. One process is performed at ambient temperature, which requires residence times in the range of minutes and a second method operates at elevated temperatures of up to 200 °C during the coating formation, requiring residence times of only a few seconds. While TEOS can be used in both, HMDSO requires the more reactive environment at elevated temperatures.

In the present work, highly agglomerated model Pt particles, produced in a spark discharge generator (SDG), are modified with a thin silica or silica-organic coating in the post-discharge process. The mechanical stability of these particles is quantified in a low pressure impactor by impaction onto a surface and the subsequent analysis of the deposited particles. It will be shown that these coatings improve the rigidness of the agglomerates by reducing the degree of structural changes. The aim of the work is not to provide a conclusive model of the impaction and cohesion physics, but instead to demonstrate a relatively simple way to modify and study the mechanical stability of nanoparticles.

2. Material and methods

The experimental setup can be divided in two main parts. The first one comprises the particle synthesis and the subsequent coating of these particles, while the second part concerns the stability measurement. Particles were synthesized with a spark discharge generator and then coated with a plasma assisted CVD process. The stability measurements were conducted with a low pressure impactor. Fig. 1 shows an overview of the setup. Both parts of the setup were coupled and enabled the direct measurement of the coated aerosol without any intermediate steps. However, while the particles were synthesized and coated at ambient pressure (1 bar), the stability measurements required low pressures. The transfer between the pressure regimes was accomplished with a critical orifice at the inlet of the impactor. Earlier studies with the setup have shown that the sheer forces acting on the particles in this critical orifice are too small to fragment the Pt agglomerates (Gensch & Weber, 2014).

2.1. Particle synthesis and coating

The particles were continuously produced in a spark discharge generator (SDG) (Tabrizi, Ullmann, Vons, Lafont, & Schmidt-Ott, 2009). A spark discharge generator produces particles by ablation of electrode material and subsequent particle nucleation and condensation in the gas-phase (Feng et al., 2016). Platinum was used as particle material, since the produced primary particles were typically small (single digit nm) and agglomerated quickly to much larger fractal structures with thin and long branches. This

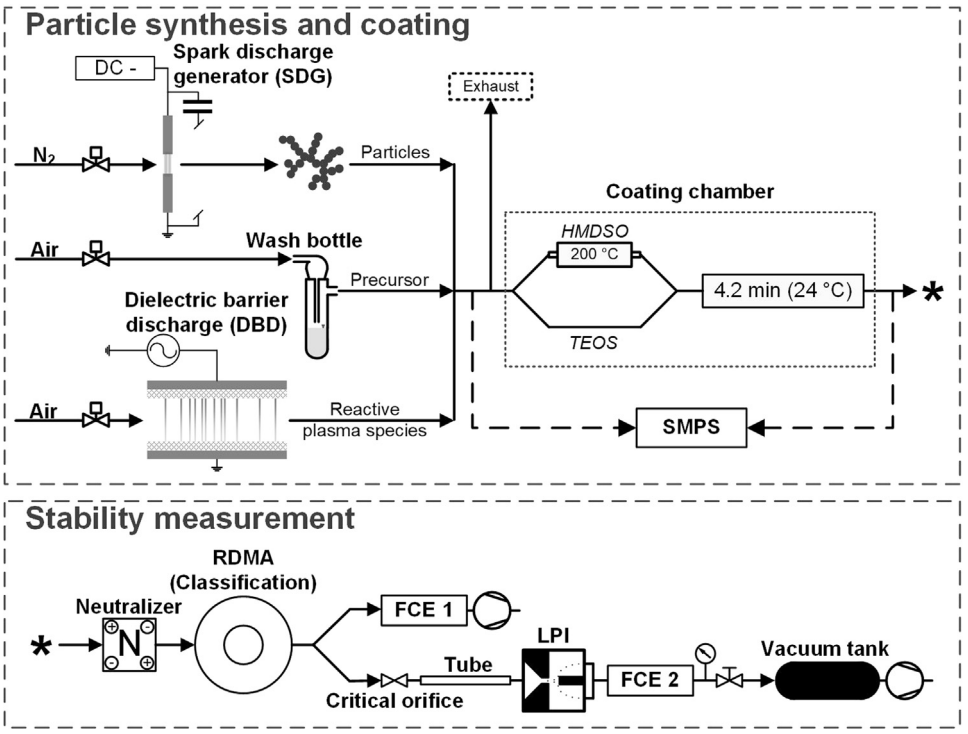

Fig. 1. Overview of the experimental setup with the two main parts particle synthesis and coating and stability measurement. SMPS: Scanning mobility particle sizer (not connected during stability measurements), RDMA: Radial differential mobility analyzer, FCE: Faraday cup electrometer, LPI: Low pressure impactor.

morphology made them interesting as model materials for stability measurements, since such dendritic structures are inherently prone to fragmentation during impaction. The particles were produced in 1 l/min nitrogen (N_2, 99.999%). A capacitor of 24 nF was used in the SDG with a charging current of 0.8 mA, which provided particle size distributions well suitable for the experiments. The distance between the Pt electrodes (99.99%, 3 mm diameter) was about 2 mm.

The plasma assisted coating process consists of the precursor addition, the production of reactive plasma species and a coating chamber, where residence time and temperature are controlled. As precursors tetraethyl orthosilicate (TEOS) and hexamethyldisiloxane (HMDSO) were used. The liquids were kept in a small washing bottle, with TEOS at 9 °C or ambient temperature (24 °C) and HMDSO at 6 °C. A small volumetric flow of air in the range of ml/min was saturated with the precursor and introduced into the system. The reactive species used to facilitate the CVD reactions were produced in a dielectric barrier discharge. The self-built reactor had a symmetric plate-to-plate geometry with an electrode area of 729 mm^2, a discharge gap of 1 mm and two alumina dielectrics of 2 mm thickness each. It was operated with 2 l/min filtered air and primarily produced ozone and different nitric oxides as longer living species. For the coating with TEOS, the particles, precursor and plasma species were mixed and then introduced into a glass tube with a volume of about 4.2 l at ambient temperature. The average residence time was kept constant at 4.2 min with a volume flow of 1 l/min through the coating chamber (laminar flow). HMDSO-based coatings were acquired by heating the aerosol in a tube furnace (200 °C) during a residence time of about 4 s. To make sure that the HMDSO-based coatings were completely hardened before the stability measurements, an additional residence time of 4.2 min at ambient temperature was added after the furnace. Particle number size distributions were measured by connecting a Scanning mobility particle sizer (SMPS, Grimm 5.403 CPC + Grimm 55-40-26-Uni DMA) and neutralizer (TSI, model 3088) either before or after the coating chamber. The SMPS was not connected during the stability measurements.

2.2. Stability measurement

The coated particles were introduced into the stability measurement setup. The particles were charged to a Boltzmann charge distribution in a soft X-ray neutralizer (TSI, model 3088) and subsequently classified according to their mobility in a radial DMA (RDMA, self-built). After classification of the desired mobility equivalent diameter, which was kept constant for all measurements at 73 nm, the aerosol flow of 1.0 l/min was split into two parts. 0.7 l/min were pumped through a Faraday cup electrometer (FCE) to monitor the particle concentration before the impaction and the rest (0.3 l/min) was introduced into the low pressure impactor (LPI) through a critical orifice. Between the critical orifice and the LPI a 1 m long tube with an inner diameter of 24 mm was installed to equalize the free jet behind the critical orifice and to obtain more homogeneous flow conditions. The LPI separates aerosol particles in the submicron range according to their inertia due to high gas velocities in a low pressure environment. Behind the impaction plate, a

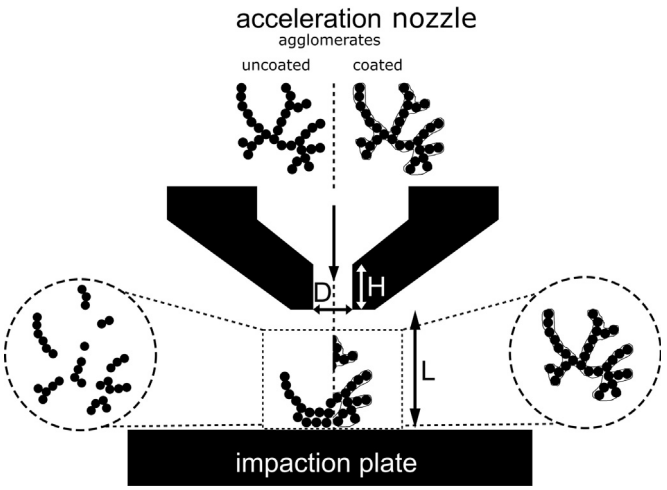

Fig. 2. Schematic display of the impactor with its characteristic geometrical parameters and the expected idealized impaction behavior of uncoated and coated agglomerates. The dotted middle line indicates symmetry and illustrates the different idealized behavior of uncoated and coated agglomerates.

second FCE was used to measure the particle concentrations leaving the LPI, which was the fraction of the aerosol particles either not deposited onto the impaction plate or bouncing back from the plate. The pressure in the LPI was measured after the second FCE and was controlled with a subsequent system of valve, gas tank and vacuum pump.

The main parts of an impactor are the acceleration nozzle and impaction plate. In all experiments, the diameter of the acceleration nozzle was 2 mm. The impaction plate was set at a 90° angle to the flow direction from the nozzle, so that the particles impacted perpendicular on the surface ("target"). An important geometrical parameter of the impactor, which describes the ratio of the distance between the acceleration nozzle and the impaction plate L to the diameter of the acceleration nozzle D, is the L/D ratio (Fig. 2). The value of the L/D ratio was 2.125 for all measurements.

The model by Rennecke & Weber (2013) was used to calculate the velocities at which the particles impacted onto the target plate. The impaction velocity U_{imp} of the particles can be calculated with the geometric dimensions of the LPI. The governing equation shows the influences of the modified Stokes Number Stk* and the geometrical values of the setup:

$$U_{imp} = \bar{U}_{imp}(Stk^*, L/D)\cdot U_{max,Gas}(p, \dot{m}_{Gas})\cdot\chi_{lag}(Stk^*, L/D, H/D)$$

$U_{max,Gas}$ is the maximum gas velocity at the acceleration nozzle outlet, which depends on the gas density and mass flow rate, χ_{lag} is a correction term, which considers the lag of the particle motion behind the gas flow due to inertia (in gas streamline direction) and $\bar{U}_{imp}$ describes the dimensionless impaction velocity, which can be calculated with the following equation:

$$\bar{U}_{imp} = \frac{-B}{Stk^* + A} + 1$$

where A and B are empirical constants, which are derived from numerical calculations and depend on the setup geometry (Rennecke & Weber, 2013).

The modified Stokes number Stk^* is defined by the maximum gas velocity U_{max} and for a parabolic stream profile in the acceleration nozzle is twice the common Stokes number, which depends on the average gas velocity $\bar{U}$. The value of Stk^* is a function of the p_{50} value, the chosen impaction pressure p_{imp} and Stk_{50} which is constant for given L/D ratios (Rennecke & Weber, 2013). p_{50} describes the pressure at which 50% of the particles are deposited on the impaction plate. Therefore Stk^* can be calculated with the following equation:

Table 1
Constants used for the calculation of $\bar{U}_{imp}$ for different L/D ratios from Rennecke and Weber (2013) and values used here (L/D = 2.125).

L/D	A	B	Stk_{50}
1	0.181	0.505	0.474
2	0.328	0.692	0.585
2.125	0.365	0.724	0.599
3	0.581	1.012	0.693
5	1.616	2.215	0.943

Table 2
Examples of values used in the calculation of the lag-factor.

p_{imp} (mbar)	Stk^*	$\bar{S}_{99}$	χ_{lag}
5	9.771	19.543	0.736
10	2.443	4.886	0.978
15	1.086	2.171	0.999
20	0.611	1.221	1

$$Stk^* = \frac{\tau \cdot U_{max,Gas}}{D/2} = 2\frac{\tau \cdot \overline{U}}{D/2} = Stk_{50} \cdot \frac{{p_{50}}^2}{{p_{imp}}^2} = 2 \cdot Stk$$

Table 1 shows the constants needed to calculate $\bar{U}_{imp}$ for different L/D ratios, which were determined by Rennecke and Weber (2013). The L/D ratio is given by the geometry of the impactor, as described in Fig. 2. The associated constants are then interpolated from the values in the table for the ratio used here (L/D = 2.125).

The lag-factor χ_{lag} is a correction function and considers the lag of the particle response to a change of the gas velocity (acceleration or deceleration). Due to the higher relaxation times and lower degree of friction in a low pressure environment, there can be a significant difference between the gas velocity and the velocity of the gas-borne particles. χ_{lag} depends also on the geometrical setup and the agglomerate size. It can be calculated with the following equation:

$$\chi_{lag} = 1 - 0.6 \cdot \exp\left(-\frac{\overline{S}/\overline{S}_{99}}{0.21}\right) - 0.4 \cdot \exp\left(-\frac{\overline{S}/\overline{S}_{99}}{0.014}\right)$$

with

$$\overline{S} = \frac{H + L}{D} - 0.5 \quad \overline{S}_{99} = 2 \cdot Stk^*$$

$\bar{S}$ is defined as the actual available acceleration distance and $\bar{S}_{99}$ is the distance necessary for complete acceleration of the particles to the gas velocity. The available distance solely depends on the geometrical dimensions of the impactor, while the necessary distance will increase with decreasing pressure As an example, Table 2 shows the lag-factor at varying pressures for one sample.

In this work, the stability of the particles is related to the degree of fragmentation during impaction. This was characterized by a change in the projection area of the particles deposited on the impaction plate, which was obtained from TEM micrographs. The loaded TEM grids were analyzed using a JEOL JEM2100. To collect samples for TEM analysis, a TEM grid was positioned in the center of the impaction plate with no voltage applied to the RDMA. Then the voltage was applied to the RDMA to obtain particles of a constant mobility equivalent diameter. The equivalent diameter was kept constant for all experiments, close to the mode diameter of the particle size distribution of the unmodified particles. During the TEM sampling, the pressure in the LPI was kept constant at a value corresponding to the desired impaction velocity. The sampling time was between one and four minutes for every experiment, depending on the FCE signal output. The sampling time was adjusted in the way that enough particles were deposited on the sample grid for a good statistical analysis by TEM, without overloading the TEM grid with agglomerates. The fraction of deposited particles depends on the impaction velocity with a higher velocity resulting in a higher degree of deposition. However, at high impaction velocities, the impaction area was focused, which could result in agglomerates impacting onto already deposited ones (Rennecke & Weber, 2013). Therefore, to avoid the risk of overloading the sampling time was reduced when focusing effects were encountered. For each sample, 50 micrographs, containing at least one particle each (more for the higher velocities with many small fragments), were acquired at random grid positions and their projection area was subsequently analyzed with ImageJ. This image analysis followed the same steps every time to guarantee comparable data. First, the scale was transferred from the TEM micrographs into ImageJ. The micrographs were then transformed into binary images, where the particles were black and the background white. It was ensured that no parts of the particles were added (dilation) or subtracted (erosion) in this step. The transformed images were used to automatically determine and outline the areas of the particles in the images. In a final step, the output files with the outlines were compared with the original micrographs to ensure that every particle was recognized correctly. The raw data was then further processed to get the data and error bars seen in the Figs. 9 and 11, as described in Appendix.

3. Results and discussion

3.1. Structure of the model particles

The model particles were produced with a spark discharge generator, using Pt electrodes. The primary particles produced in the SDG were very small, with diameters in the single digit range (about 3–4 nm), but agglomerated quickly, due to high number concentrations, to much larger structures with mobility equivalent diameters between 20 and 100 nm. Because of the Brownian motion, the agglomerates were dendritic, with long and thin particle branches randomly oriented. These branches are not rigid and will, for example, vibrate heavily in the electron beam of the TEM, which indicates some fragility. Fig. 3a shows an unmodified Pt agglomerate deposited on a TEM grid by diffusion after passing the RDMA. Parts of the agglomerates stand up from the substrate after diffusional deposition or inertial deposition at low impaction velocities. These branches can be identified by their vibration during

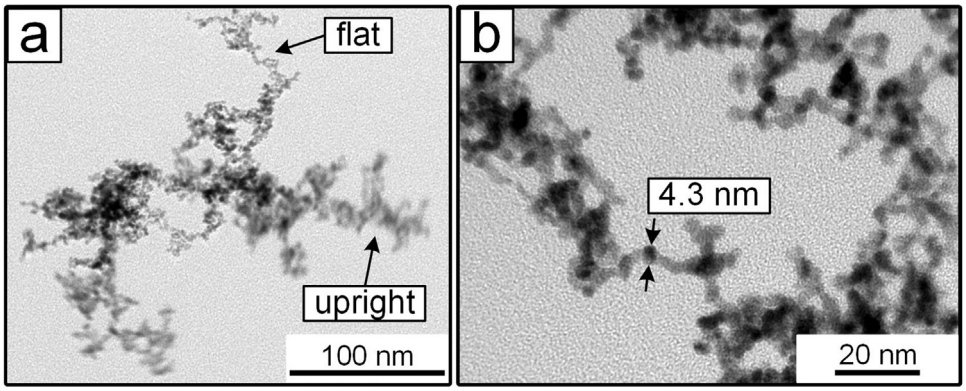

Fig. 3. Structure of diffusion deposited Pt agglomerates. Agglomerates deposited by diffusion or low impaction velocities exhibit a certain amount of branches not lying flat on the substrate (a). The individual primary particles are around 3–4 nm in diameter and seem to be primarily connected by solid bridges (b).

TEM analysis and the different focusing plane resulting in blurry micrographs (Fig. 3a). The fractal dimension of these Pt agglomerates was determined by previous impactor measurements to be around $D_f = 1.8$. The individual primary particles seem to be primarily connected by sintering bridges and are hard to distinguish from their neighbors (Fig. 3b). In many cases, the agglomerate branches consist of multiple parallel particle-particle connections. However, in other parts of the agglomerates, only single particle bonds are observed, which are presumably the weakest parts in the structure (Fig. 3b).

Fig. 4 shows the particle number size distributions for the unmodified agglomerates, measured before and behind the coating chamber (residence time of 4.2 min). During the transit through the coating chamber, the particle number distribution changed even without applying a coating. The distribution was shifted to larger particle sizes and the particle number concentration decreased. As shown before (Post & Weber, 2018), these changes are mainly caused by agglomeration of the particles, with diffusion losses to walls having a smaller influence.

The two different precursors used for coating purposes in this work required different temperatures during the process. While the experiments with inorganic silica coatings from TEOS were performed at ambient temperature, the use of HMDSO required the heating of the aerosol to 200 °C for a few seconds. A Pt agglomerate impacted on the TEM grid after 4.2 min transit time is shown in Fig. 5a. The low impaction velocity (15 m/s) seemed to cause no significant structural changes compared to the diffusional deposition, as indicated by the close agreement of mobility (73 nm) and projection area equivalent diameters (81 nm) (Rogak, Flagan, & Nguyen, 1993). The tempering for the HMDSO coatings is expected to influence the form of the Pt agglomerates, due to a beginning restructuring to more compact structures, even though the actual melting point of the materials is much higher. This effect is typically observed for weakly bonded structures (Weber & Friedlander, 1997). An example for a more compact agglomerate is shown in Fig. 5b. Therefore, in case of fragmentation experiments with HMDSO coatings, the uncoated Pt agglomerates were exposed to 200 °C for the same duration as the coated ones to obtain comparable initial agglomerate structures.

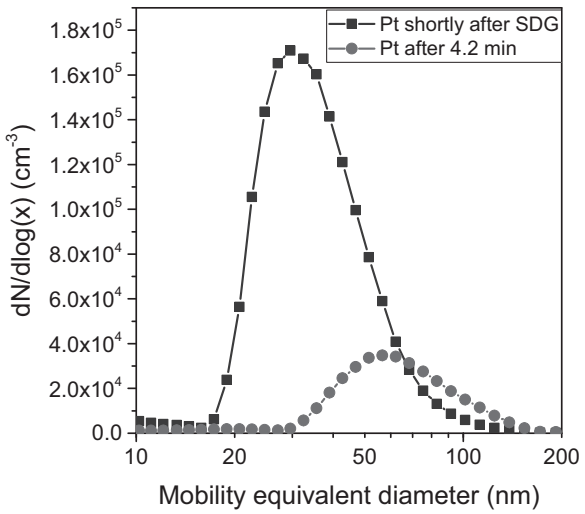

Fig. 4. Particle size distribution of the original spark discharged generated platinum agglomerates and of the agglomerates after a residence time of 4.2 min.

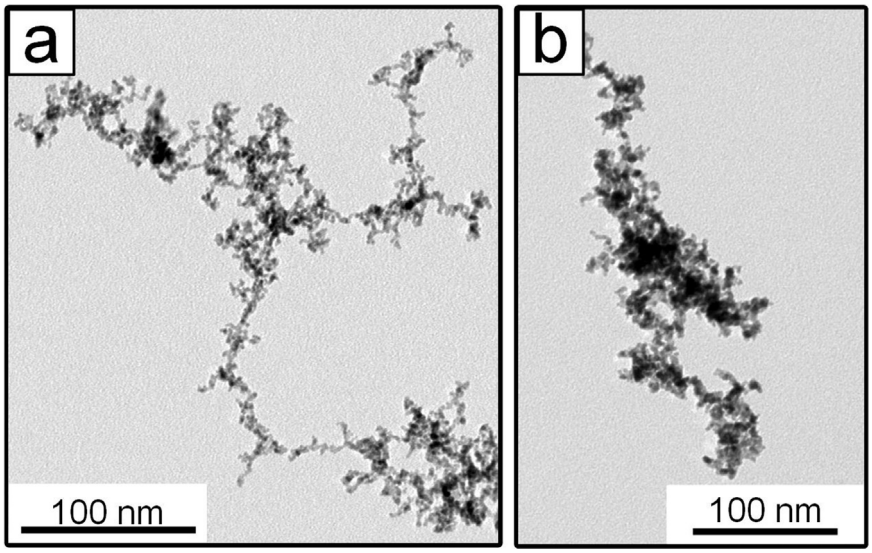

Fig. 5. Uncoated Pt agglomerates (about 80 nm projection area equivalent diameter), impacted onto the TEM grid at about 15 m/s. After a residence time of 4.2 min at ambient temperature (a). After 4 s at 200 °C and subsequent 4.2 min at ambient temperature (b).

Depending on the precursor, also the finished coatings on the agglomerates exhibit differences. As mentioned before, the coatings using TEOS as precursor are typically inorganic in nature (SiO_x with x being close to 2). The HMDSO-based coatings, on the other hand, contain more organic bonds, such as Si-CH_3. This can be observed macroscopically with the sessile drop method as a change of the particle wetting behavior from hydrophilic to hydrophobic (Post, Wurlitzer, et al., 2018). Hence, the intermediate products present during the coating formation are presumably also more hydrophilic in the case of TEOS and hydrophobic for HMDSO. For thicker HMDSO coatings, this often results in less homogeneously distributed coating material on the metal particles, since the coating intermediates seem not to be able to wet the structures as well as the TEOS intermediates. However, for thin coatings such as those used in this work, this effect seems to be negligible since the resulting coatings appear similarly homogeneous as the TEOS ones in TEM micrographs (Fig. 6). While the coating mechanisms are not completely understood and beyond the scope of this work, it could be speculated that this might indicate a dominance of surface reactions in this concentration range in contrast to one of gas-phase reactions with subsequent condensation at higher concentrations. Fig. 6 shows examples of Pt agglomerates coated with the two precursors. The coatings shown are somewhat thicker than those used in the fragmentation experiments to illustrate the discussed effects better. The coatings tend to accumulate in the inner parts of the agglomerates (e.g. arrows in Fig. 6), while outer primary particles often exhibit locally thinner coatings. For even thinner coatings with too little coating material to cover the agglomerate surfaces completely, the coatings will primarily form in these parts, but not exclusively. This might be related to capillary forces acting on liquid coating intermediates.

3.2. Rebound and deposition behavior of the agglomerates

Particles impacting on the TEM grid can rebound from the impaction plate into the carrier gas and leave the LPI setup. This is observed when the kinetic energy of the impacting particle cannot completely be dissipated in deformation processes. Instead, an

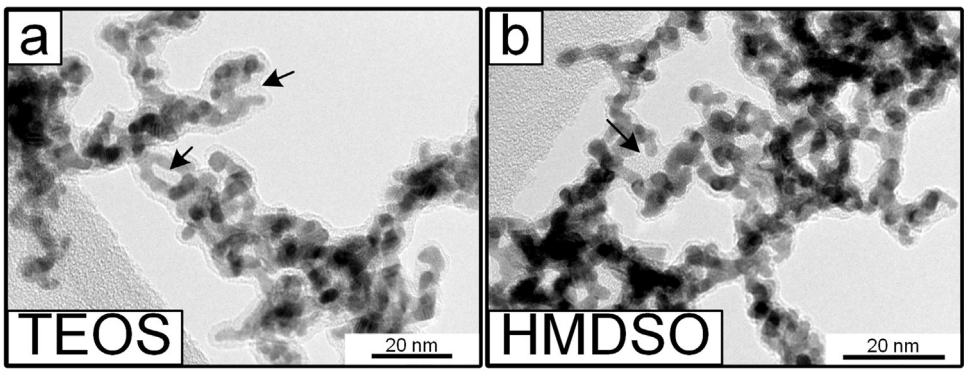

Fig. 6. Examples of Pt agglomerate parts coated with TEOS (a) and HMDSO (b). The coatings shown are somewhat thicker than those used in the rest of this work to make the coatings more visible. The arrows show examples of coating accumulation.

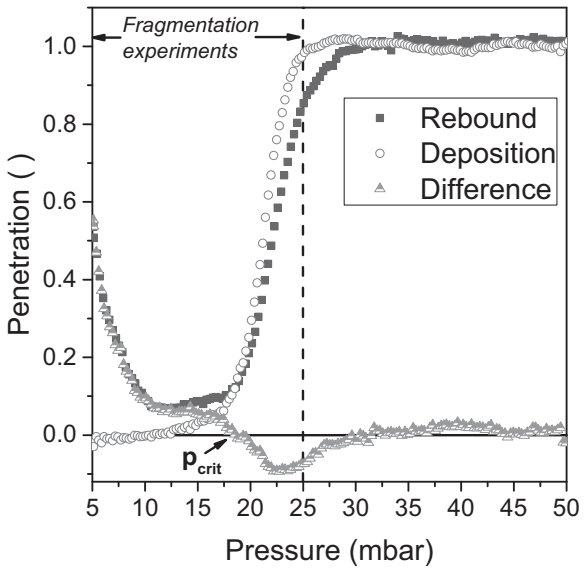

Fig. 7. Measurement of the rebound behavior of silica-coated Pt particles (atomic ratio Si/Pt = 0.39). The penetration is the ratio of the particle concentration leaving the LPI to the initial one. The pressure range in which the fragmentation experiments for these particles were conducted is indicated.

elastic part of it is converted back into kinetic energy, which leads to rebound if the elastically stored energy of the impacting particle is larger than the adhesion energy between the particle and the substrate. The onset of particle bounce depends on the substrate as well as the particle material. Harder, more rigid materials impacting on smooth and hard surfaces will rebound more easily than deformable materials impacting on deformable surfaces. The rebound of particles from the impaction plate can obviously not be measured with the TEM method used in the other sections, since the particles do not remain on the grid. However, the rebound can be obtained from the FCE measurements. As an example, the rebound behavior of the TEOS-coated particles with the thinner silica coating (Si/Pt = 0.39 in Fig. 9) on a TEM grid is shown in Fig. 7. Most of the other samples behaved very similarly (cf. Fig. 8).

The rebound experiment consisted of two parts: the deposition measurement and the rebound measurement. In both cases, the particle penetration was measured as the ratio of the particle concentration after the LPI to the particle concentration prior to the impactor. Both were measured with FCEs and the pressure in the LPI was recorded simultaneously. For the deposition measurement, the rebound from the surface was suppressed with a greased sticky substrate, which greatly improved the energy dissipation, deformation and adhesion energy between agglomerate and surface. This resulted in the so-called deposition curve (Fig. 7). For the rebound measurement, the TEM grid was placed on the impaction plate in the same manner as in the fragmentation measurements. Particles can rebound from this surface and return to the gas flow. In contrast to the fragmentation measurements, the data recording for both deposition and rebound was carried out by continuously scanning a pressure range instead of multiple constant pressures. A lower pressure corresponds to a higher impaction velocity. The evacuated gas tank was filled through the LPI setup during the measurement, which resulted in a continuously decreasing impaction velocity. The difference between deposition and rebound measurements describes the bounced fraction (Gensch & Weber, 2017; Rennecke & Weber, 2013). The indicated critical pressure p_{crit} is the pressure where bouncing starts. For the measurements shown in Fig. 7, p_{crit} was 18.1 mbar, which corresponds to a critical velocity of 57 m/s. Furthermore, after a plateau at around 15–10 mbar there seems to be an increase in rebound at a pressure below 8 mbar. This is equivalent to an impaction velocity of around 220 m/s.

The pressure range corresponding to the velocities used in the fragmentation experiments of this sample (Section 3.3) is indicated in the figure. It shows that rebound of particles will occur in parallel to the structural changes. The amount of particles deposited on the TEM grid depends on the impaction velocity. Low velocities result in fewer particles available for analysis, due to a penetration close to one. This necessitates a longer sampling time for these impaction velocities to guarantee enough particles, while a low degree of penetration might overload the TEM grid and hence requires shorter sampling times. However, as shown by Ihalainen et al. (2012), the size distribution of particles deposited on an impactor target is very similar to that of particles collected after the impactor, even when rebound is observed. Hence, the rebound of some agglomerates should not influence the results in this work.

Coatings on particles influence the mass of the resulting composite and hence might change their inertia and impaction behavior. The calculation of the impaction velocity takes this into account by using the p_{50} value of the respective agglomerates (Section 2.2). For a given impactor geometry, the positions of the deposition curves and the corresponding p_{50} values, where 50% of the particles are deposited, are influenced by the effective density of the agglomerates. The effective density is the ratio of the particle mass to its aerodynamic volume (Seipenbusch, Heel, Weber, & Kasper, 2002). The deposition curves for the different coating conditions are shown in Fig. 8.

The comparison of the different coating thicknesses for TEOS at 24 °C shows a shift of the curves to slightly higher pressures with increasing coating amount. This is expected, since coatings on inner parts of size classified agglomerates increase their effective

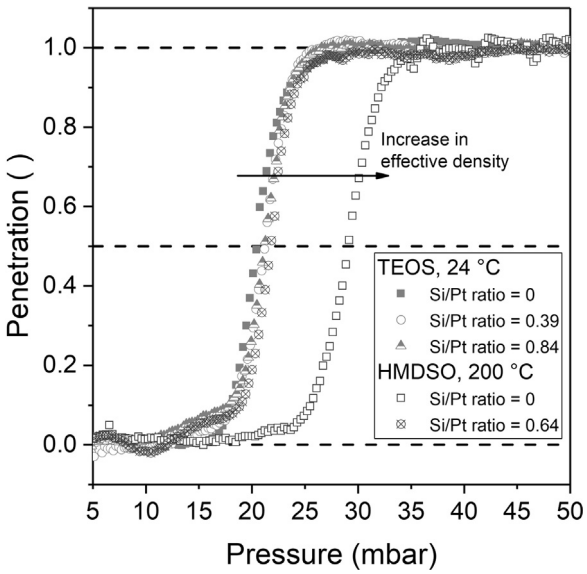

Fig. 8. Deposition curves of the agglomerates in the impactor in dependence on the coating conditions. The positions of the curves relate to the effective density of the particles.

density but hardly their projection area (Seipenbusch et al., 2002). Furthermore, the small differences between the coating thicknesses indicate that the coated particles impact hardly differently than the uncoated particles and only their fragmentation behavior might be different. This shows that no significant structural changes were caused by the coating process. This situation is different for the particles tempered in the tube furnace at 200 °C and coated with HMDSO. Here, clear differences between the coated and uncoated particles are apparent. The deposition curve of the uncoated particles is shifted to a higher pressure compared to those at 24 °C (p_{50} from 20.5 to 29 mbar), which indicates structural changes caused by the tempering. However, the HMDSO-coated particles behaved very similar to the TEOS-coated particles, even though they experienced higher temperatures. This indicates that the coating counteracts the restructuring of the particles, which is also apparent in their fragmentation behavior (Section 3.4).

3.3. Impaction of silica-coated Pt particles

Pt agglomerates were coated with silica using TEOS precursor at ambient temperature and introduced into the stability measurement setup. The impaction velocity was varied via the pressure in the impactor and the projection area of the agglomerates was determined with ImageJ from TEM micrographs of particles deposited on the sample grid on the impaction plate. The coating amount was controlled by the initial TEOS concentrations of 0.3 and 1.5 ppmv, respectively. These coating conditions were chosen to acquire thin coatings on the particles to simulate a change in the mechanical stability without a complete passivation of the core particle surfaces. In the branched structures of the Pt agglomerates, the thin coatings tended to accumulate in the areas between primary particles. This made it difficult to determine a meaningful coating thickness from TEM micrographs. Instead, the amount of coating was analyzed by EDX in the TEM and is given as the ratio of the atomic percentages of Si to Pt. A higher ratio indicates a thicker or more complete coating. Fig. 9 shows the results of these measurements. The uncoated Pt particles followed the same pathways through the inactive coating setup as the coated particles to guarantee equal residence times and agglomeration before the measurement. Within a sample, the equivalent diameters could vary significantly. This is expected for this kind of fragmentation analysis with such dendritic particles and was observed before (Gensch & Weber, 2014).

The TEM micrographs show the differences between the structures of the impacted uncoated agglomerates for four velocities with smaller fragments present at the higher velocities (Fig. 9). Going into more detail, the equivalent diameter of the uncoated Pt particles (Si/Pt = 0) showed a significant increase from an initial value of about 81 nm at 16 m/s to 94 nm at 36 m/s. Between 59 and 89 m/s, the diameter decreased below the initial value, indicating a fragmentation of the agglomerates, with the fragment size decreasing with higher velocities. At 255 m/s impaction velocity a remaining diameter of 13 nm was measured. Simultaneously, the number of fragments should increase, which, however, cannot be measured by TEM. Most of the agglomerates did not fragment into individual primary particles (about 4 nm) in the studied velocity range. The significant increase in diameter in the intermediate velocity range (between 16 and 60 m/s) is counterintuitive at first, since it seems to show that the agglomerates increase in size during the impaction. However, this is probably an effect of the measurement method, which represents a 3-dimensional agglomerate as a 2-dimensional image as discussed in the following.

Two effects might influence the area equivalent diameter of the impacted particles simultaneously. A depiction of the possible structural changes experienced by an agglomerate impacting on a surface is shown in Fig. 10. The Pt agglomerates approach the TEM grid on the impaction plate with the impaction velocity, depending primarily on the gas velocity and the particle inertia (a). When the particles impact on the substrate, they experience deceleration forces that will stress the binding forces between the primary particles.

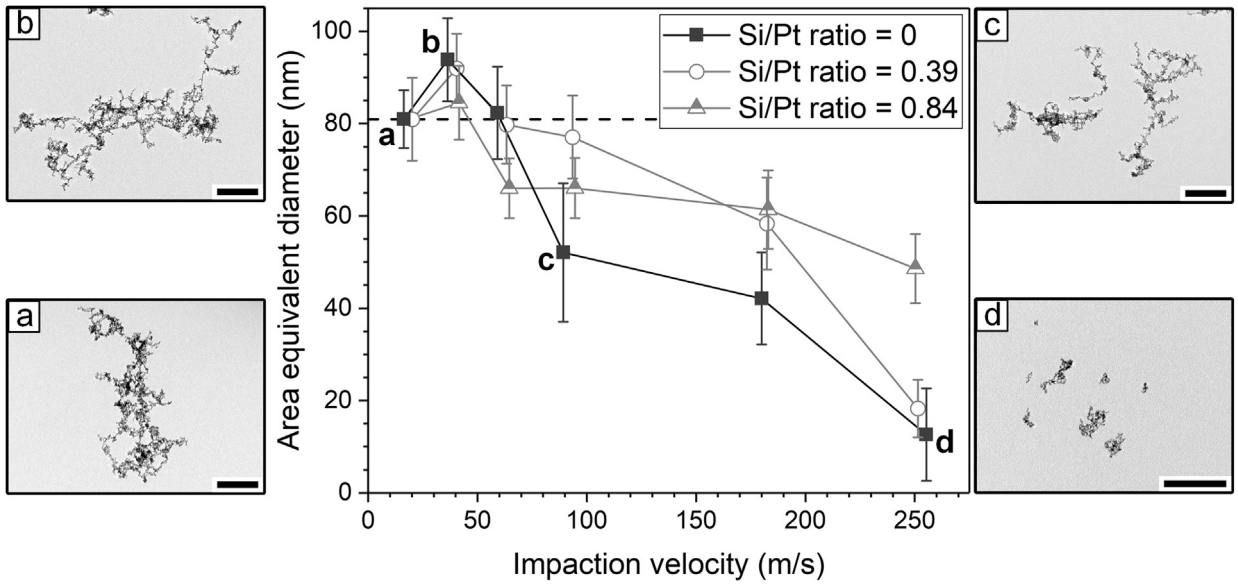

Fig. 9. Changes in the area equivalent diameter of Pt agglomerates in dependence on their impaction velocity. The particles were coated with silica coatings with the post-discharge process using TEOS. Si/Pt indicates the relative amount of coating on the particles and was calculated from EDX measurements. Si/Pt = 0 indicates uncoated particles. The TEM micrographs correspond to the uncoated particles. The lengths of the black bars correspond to 100 nm. The lines between the data points were added as a guide to the eye.

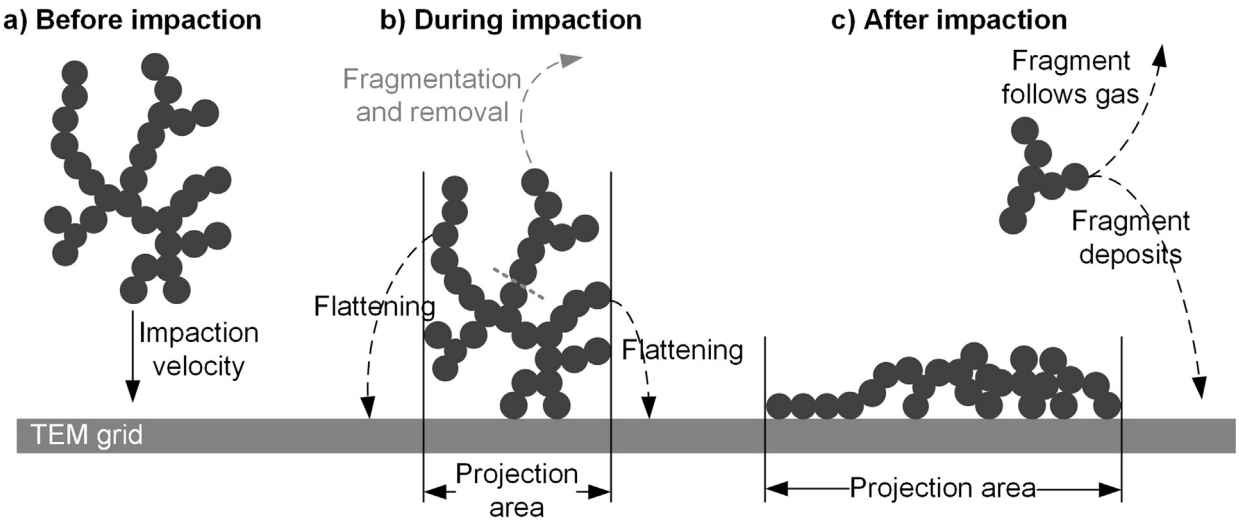

Fig. 10. Possible effects of the impaction on the agglomerate structure.

This can result in either a restructuring of the particles without separation from the main agglomerate or a fragmentation of agglomerate parts (b). The exact phenomena causing the fragmentation of agglomerates are complex and only shown simplified in Fig. 10. The fragments could either follow the gas out of the impactor or deposit somewhere on the TEM grid (c). It is also possible for agglomerates or fragments to bounce away from the substrate surface after impaction, as shown in Section 3.2. With regard to the measured parameter, the projection area, a flattening of the agglomerate onto the substrate can result in an increase in the measured area, while fragmentation decreases the projection area of individual agglomerates. The ratio of fragmentation to flattening seems to depend significantly on the impaction velocity. Lower impaction velocities favor the flattening of branches without breaking, while higher velocities result in the breakage of interparticle bonds. Very small velocities result in a mainly diffusional deposition and no significant changes of the particle structure. Here, branches of the deposited agglomerates protrude from the surface, as discussed before (Section 3.1).

In contrast, the coated particles showed a different behavior (Fig. 9). Between 16 and 60 m/s the equivalent diameter increased for the coated particles, likely due to the flattening effect. However, while the increase for the lower coating amount (Si/Pt = 0.39) was similar to that of the uncoated particles, the thicker coating (Si/Pt = 0.84) resulted in a much smaller increase. This indicates

that the thicker coating improved the rigidness of the protruding branches. Many of the branches seemed no longer flexible enough to flatten to the TEM grid and instead stood upright until the impaction velocity was high enough to fragment the modified structure. However, the fragmentation at higher velocities was reduced in comparison to the uncoated agglomerates for both coated agglomerates. While the diameter of the thinly coated agglomerates followed a linear downwards trend, the thicker coating resulted in a flatter progression after an initial decrease between 40 and 65 m/s. It also resulted in much larger structures at the highest velocity of about 250 m/s (49 vs. 13 and 18 nm), indicating strong cohesion between the remaining agglomerate parts. The smaller diameters of the thicker coating (Si/Pt = 0.84) in comparison to the thinner coating between about 63 and 180 m/s point to a decrease in stability of some agglomerate parts in the thicker coated particles. This could correspond to the agglomerate branches in those agglomerates that do not flatten during the low impaction velocities. Even though a coating is applied, these structures are presumably still weaker than the more compact parts of the particles. Especially since incomplete coatings tend to accumulate in the inner parts of complex structures (Post et al., 2016). While the thicker coating increased the rigidness of the branches, as shown by the lower degree of flattening, the branches are presumably still the easiest parts to break. When the impaction velocity crosses an energy threshold, these parts might fragment directly instead of restructuring first, due to their coating-restrained flexibility. Remaining parts of the agglomerates would then be more compact and will not fragment much further, resulting in the low subsequent reduction in diameter. In contrast, the thinner coating (Si/Pt = 0.39) seems to slow down the fragmentation in comparison to the uncoated particles, but not prevent it completely. Overall, the results seem to demonstrate that the coatings can be used to stabilize particles mechanically against restructuring by impaction. The effect might be comparable to an increase in cross-sectional area of sintering necks due to higher sintering temperatures as observed by Seipenbusch et al. (2010). In the present work, the cross-sectional area is obviously not increased by changes of the core material, but instead by the additional coating material deposited on the agglomerates.

3.4. Impaction of silica-organic-coated Pt particles

Alternatively, the Pt particles were coated with the second silicon precursor, HMDSO. This resulted in more organic silica coatings ($SiO_xC_yH_z$), compared to the inorganic coatings with TEOS (SiO_x). Furthermore, the coating process with HMDSO necessitated the heating of the aerosol and precursor mixture to 200 °C for about 4 s prior to the 4.2 min at ambient temperature. While the resulting thermal stress was not enough to sinter the particles, they restructured to agglomerates that were more compact, as shown before (Fig. 5). This seemed to influence the stability of the uncoated agglomerates. In contrast to the uncoated particles at ambient temperature (Fig. 11, Si/Pt = 0 (24 °C)), those restructured at 200 °C (Fig. 11, Si/Pt = 0) showed no increase in area equivalent diameter between 16 and 60 m/s and instead a significant diameter decrease in this velocity range. Due to the tempering, the agglomerates seemed to have a lower amount of protruding branches, which removed the flattening effect from the measurements. However, there still seemed to be some parts of the agglomerates that were only connected by single particles to the rest of the structure (e.g. Fig. 5b, top part). These particle bonds might be the weak points of the structures, resulting in fragmentation in the velocity range where flattening was observed before. The tempered particles showed a strong degree of fragmentation above 100 m/s

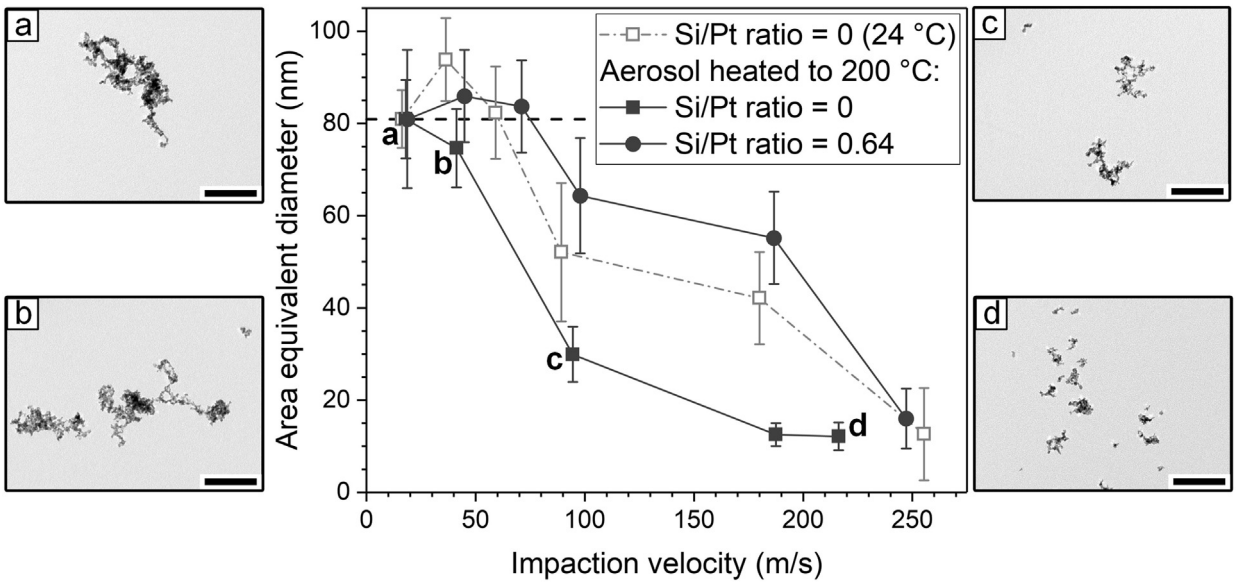

Fig. 11. Changes in the area equivalent diameter of Pt agglomerates in dependence on their impaction velocity. The particles were coated with silica-organic coatings with the post-discharge process at 200 °C using HMDSO. Si/Pt indicates the relative amount of coating on the particles and was calculated from EDX measurements. Si/Pt = 0 indicates uncoated particles. Si/Pt = 0 (24 °C) are the original agglomerates shown in Fig. 9. The TEM micrographs correspond to the uncoated particles at 200 °C. The lengths of the black bars correspond to 100 nm. The lines between the data points were added as a guide to the eye.

with projection areas as low as 12 nm. However, the compacted inner parts of the tempered agglomerates seemed to remain largely unchanged even at high impaction velocities. The median value does not show this, since the number of small fragments was very high in comparison to the larger parts. These compacted parts seemed to be quite resilient against restructuring.

Interestingly, the coated particles (Fig. 11, Si/Pt = 0.64) showed a quite different behavior than the uncoated tempered agglomerates. In fact, the area equivalent diameter progression seems more similar to the particles without tempering (Fig. 11, Si/Pt = 0 (24 °C)). An increase in equivalent diameter from 81 to 86 nm was observed for the coated agglomerates between 18 and 70 m/s, which indicates the flattening effect. This could be related to the partial hampering of the thermal restructuring by the simultaneously occurring coating formation, leading to more remaining protruding branches in the agglomerates. The subsequent curve progression seems similar to that observed for the TEOS-coated particles as well. The diameter decreases above 70 m/s, but much less than for the uncoated and tempered particles. It seems to flatten out between 100 and 185 m/s at a much higher level (about 60 nm) than the corresponding uncoated particles (about 20 nm) before it decreases to a similar value as that observed for the uncoated tempered particles of 16 nm at 245 m/s. This might indicate different degrees of particle cohesion in the coated agglomerate. During the first decrease around 100 m/s, weakly bonded agglomerate parts separate, which were possibly left uncoated. This leaves behind the more strongly bonded agglomerates that require the higher impaction velocities above 185 m/s for further fragmentation. The hampering of the restructuring by the coating is also corroborated by the deposition behavior shown earlier (Section 3.2). Overall, the coating with HMDSO seems to have a similar effect to the one with TEOS, even though the chemical composition and coating environment are different.

4. Conclusion

A low pressure impactor was used in combination with TEM image analysis to study the size of deposited agglomerate fragments and the rebound behavior of particles. Spark discharge generated Pt agglomerates were used as model particles and coated with different silica coating materials and thicknesses in a plasma assisted CVD process at ambient or elevated temperature. Different effects seem to influence the projection area equivalent diameter of impacted particles, which was taken as indicator for the agglomerate size, such as the flattening of protruding agglomerate branches and fragmentation of agglomerate parts. When starting from low impaction velocities, increasing the velocity resulted first in the flattening of the long and fragile agglomerate branches onto the TEM grid, which was observed as an increase in the diameter. At higher velocities, the fragmentation of agglomerates into smaller particles took over, resulting in a decrease of the equivalent diameter. It was found that the coatings seemed to improve the structural integrity of the agglomerates, which reduced the influence of the flattening and lowered the degree of fragmentation. A higher amount of coating material on the particles improved this effect further. When the uncoated agglomerates were exposed to higher temperatures of 200 °C for a few seconds, they exhibited no flattening and instead fragmented early, indicating a compaction of the structure and changes to the primary particle cohesion by the tempering. This structural changes were also observed in the deposition behavior of the particle in the impactor. The silica-organic coating applied during the aerosol heating resulted in less fragmentation at intermediate impaction velocities compared to the uncoated particles exposed to this temperature. During deposition experiments, the silica-organic-coated particles also showed behavior more similar to the agglomerates kept at 24 °C. Finally, the particle bounce was studied for the experimental conditions and it was found that particle bounce occurs during the impaction on the TEM grid.

Acknowledgements

This work was supported by the Deutsche Forschungsgemeinschaft (DFG) [grant number WE 2331/18-1].

Conflicts of interest

The authors declare no conflict of interest.

Appendix

Processes like comminution and fragmentation lead inherently to broad “daughter” distributions even when the “mother” particles have a narrow size distribution. In comminution this is a consequence of distributed strength (differences in fracture mechanics) and distributed stressing. The situation in agglomerate fragmentation is similar with distributed bond strength and distributed impact loading. Therefore, the calculation of the normal standard deviation leads to large deviations not appropriately representing the nature of fragmentation process. Thus, in accordance with the fracture function in comminution a fragmentation function giving the size distribution of the fragments was defined. Together with the probabilities of fragmentation given by the following equation, this fragment size distribution allows for the complete and adequate description of the fragmentation process:

$$S = 1 - \exp(-fc(U_{imp}^2 - U_{start}^2))$$

S describes the degree of fragmentation, f is a material specific parameter and c gives the number of contacts in a single agglomerate, U_{start} is the velocity at which fragmentation begins and U_{imp} is the impaction velocity (Gensch & Weber, 2014).

While for comminution Vogel and Peukert (2005) proposed a cumulative fracture function using tanh(x), we found that for fragmentation the cumulative size distribution for impaction fragments of nanoparticle agglomerates is fitted best with the following

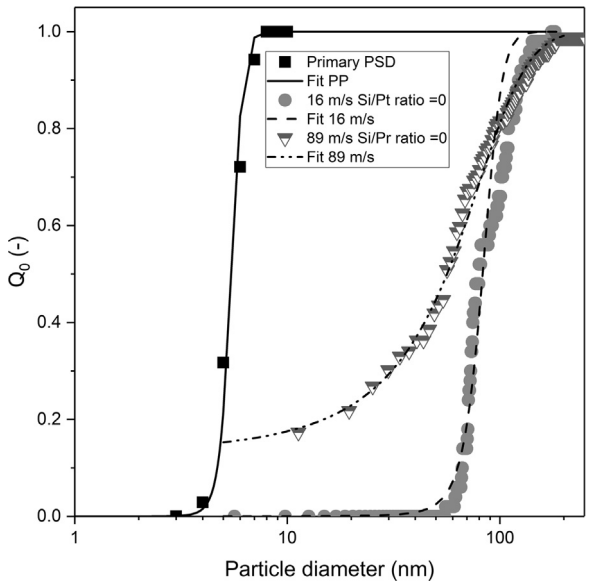

Fig. A. Exemplary data for fragment size distributions of the uncoated agglomerates (24 °C) at different impaction velocities and the primary particles size distribution (PSD) as comparison.

function:

$$B(x) = [1 + \exp(-\frac{(x - x_M)}{\Delta x})]^{-1}$$

where x is the fragment size, xM is the median fragment size and Δx is the width of the distribution.

To be able to fit these function to the gathered data, the projection area values were transformed into area equivalent diameters and plotted as Q0 sum distributions. Fig. A displays exemplarily data for the fitted fragment size distributions of different impaction velocities. With increasing impaction velocity, the fragment distributions shifts to the left (closer to the primary particles) or to the right when the flattening effect is observed. To show this in the results of this work, the widths of the distributions were used as the error bars in Figs. 9 and 11.

References

Eggersdorfer, M. L., Kadau, D., Herrmann, H. J., & Pratsinis, S. E. (2010). Fragmentation and restructuring of soft-agglomerates under shear. *Journal of Colloid and Interface Science, 342*(2), 261–268. https://doi.org/10.1016/j.jcis.2009.10.062.

Feng, J., Huang, L., Ludvigsson, L., Messing, M. E., Maisser, A., Biskos, G., & Schmidt-Ott, A. (2016). General approach to the evolution of singlet nanoparticles from a rapidly quenched point source. *The Journal of Physical Chemistry C, 120*(1), 621–630. https://doi.org/10.1021/acs.jpcc.5b06503.

Froeschke, S., Kohler, S., Weber, A., & Kasper, G. (2003). Impact fragmentation of nanoparticle agglomerates. *Journal of Aerosol Science, 34*(3), 275–287. https://doi.org/10.1016/S0021-8502(02)00185-4.

Gensch, M., & Weber, A. P. (2014). Fragmentierung von gasgetragenen Nanopartikel-Agglomeraten bei schräger Impaktion. *Chemie Ingenieur Technik, 86*(3), 270–279. https://doi.org/10.1002/cite.201300134.

Gensch, M., & Weber, A. P. (2017). Rebound behavior of nanoparticle-agglomerates. *Advanced Powder Technology, 28*(8), 1930–1942. https://doi.org/10.1016/j.apt.2017.05.003.

George, S. M. (2010). Atomic layer deposition: An overview. *Chemical Reviews, 110*(1), 111–131. https://doi.org/10.1021/cr900056b.

Guraya, H. S., & James, C. (2002). Deagglomeration of rice starch-protein aggregates by high-pressure homogenization. *Starch - Stärke, 54*(3–4), 108–116. https://doi.org/10.1002/1521-379X(200204)54:3/4<108::AID-STAR108>3.0.CO;2-2.

Ihalainen, M., Lind, T., Arffman, A., Torvela, T., & Jokiniemi, J. (2014). Break-up and bounce of TiO2 agglomerates by impaction. *Aerosol Science and Technology, 48*(1), 31–41. https://doi.org/10.1080/02786826.2013.852155.

Ihalainen, M., Lind, T., Torvela, T., Lehtinen, K. E. J., & Jokiniemi, J. (2012). A method to study agglomerate breakup and bounce during impaction. *Aerosol Science and Technology, 46*(9), 990–1001. https://doi.org/10.1080/02786826.2012.685663.

Kusters, K. A., Pratsinis, S. E., Thoma, S. G., & Smith, D. M. (1993). Ultrasonic fragmentation of agglomerate powders. *Chemical Engineering Science, 48*(24), 4119–4127. https://doi.org/10.1016/0009-2509(93)80258-R.

Lei, H., Tang, Y., Li, J., Luo, J., & Zhang, J. (2007). In situ encapsulation of copper nanoparticles by the dielectric barrier discharge. *Applied Physics Letters, 91*(11), 113119. https://doi.org/10.1063/1.2785950.

Marino, E., Huijser, T., Creyghton, Y., & van der Heijden, A. (2007). Synthesis and coating of copper oxide nanoparticles using atmospheric pressure plasmas. *Surface and Coatings Technology, 201*(22–23), 9205–9208. https://doi.org/10.1016/j.surfcoat.2007.04.091.

Nessim, C., Boulos, M., & Kogelschatz, U. (2009). In-flight coating of nanoparticles in atmospheric-pressure DBD torch plasmas. *The European Physical Journal Applied Physics, 47*(2), 22819. https://doi.org/10.1051/epjap/2009076.

Post, P., Jidenko, N., Weber, A. P., & Borra, J.-P. (2016). Post-plasma SiOx coatings of metal and metal oxide nanoparticles for enhanced thermal stability and tunable photoactivity applications. *Nanomaterials, 6*(5), 91. https://doi.org/10.3390/nano6050091.

Post, P., & Weber, A. P. (2018). Beschichtung von gasgetragenen Nanopartikeln mit SiO2 mithilfe eines plasma-unterstützten CVD-Prozesses bei Umgebungsbedingungen. *Chemie Ingenieur Technik, 90*(4), 443–450. https://doi.org/10.1002/cite.201700109.

Post, P., Wurlitzer, L., Maus-Friedrichs, W., & Weber, A. P. (2018). Characterization and applications of nanoparticles modified in-flight with silica or silica-organic coatings. *Nanomaterials, 8*(7), 19.

Qi, F., Moiseev, A., Deubener, J., & Weber, A. (2011). Thermostable photocatalytically active TiO2 anatase nanoparticles. *Journal of Nanoparticle Research, 13*(3), 1325–1334. https://doi.org/10.1007/s11051-010-0211-0.

Rennecke, S., & Weber, A. P. (2013). A novel model for the determination of nanoparticle impact velocity in low pressure impactors. *Journal of Aerosol Science, 55*, 89–103. https://doi.org/10.1016/j.jaerosci.2012.07.014.

Rogak, S. N., Flagan, R. C., & Nguyen, H. V. (1993). The mobility and structure of aerosol agglomerates. *Aerosol Science and Technology, 18*(1), 25–47. https://doi.org/10.1080/02786829308959582.

Seipenbusch, M., Heel, A., Weber, A. P., & Kasper, G. (2002). Determination of coating thickness of DEHS on submicron particles by means of low pressure impaction. *Chemical Engineering & Technology, 25*(1), 77. https://doi.org/10.1002/1521-4125(200201)25:1<77::AID-CEAT77>3.0.CO;2-B.

Seipenbusch, M., Rothenbacher, S., Kirchhoff, M., Schmid, H.-J., Kasper, G., & Weber, A. P. (2010). Interparticle forces in silica nanoparticle agglomerates. *Journal of Nanoparticle Research, 12*(6), 2037–2044. https://doi.org/10.1007/s11051-009-9760-5.

Seipenbusch, M., Toneva, P., Peukert, W., & Weber, A. P. (2007). Impact fragmentation of metal nanoparticle agglomerates. *Particle & Particle Systems Characterization, 24*(3), 193–200. https://doi.org/10.1002/ppsc.200601089.

Stepien, M., Chinga-Carrasco, G., Saarinen, J. J., Teisala, H., Tuominen, M., Aromaa, M., & Toivakka, M. (2013). Wear resistance of nanoparticle coatings on paperboard. *Wear, 307*(1–2), 112–118. https://doi.org/10.1016/j.wear.2013.08.022.

Svestka, J., Cermak, I., & Grün, E. (1993). Electric charging and electrostatic fragmentation of dust particles in laboratory. *Advances in Space Research, 13*(10), 199–202.

Tabrizi, N. S., Ullmann, M., Vons, V. A., Lafont, U., & Schmidt-Ott, A. (2009). Generation of nanoparticles by spark discharge. *Journal of Nanoparticle Research, 11*(2), 315–332. https://doi.org/10.1007/s11051-008-9407-y.

Teleki, A., Heine, M. C., Krumeich, F., Akhtar, M. K., & Pratsinis, S. E. (2008). In situ coating of flame-made TiO2 particles with nanothin SiO2 films. *Langmuir, 24*(21), 12553–12558. https://doi.org/10.1021/la801630z.

Vogel, L., & Peukert, W. (2005). From single particle impact behaviour to modelling of impact mills. *Chemical Engineering Science, 60*(18), 5164–5176. https://doi.org/10.1016/j.ces.2005.03.064.

Vons, V., Creyghton, Y., & Schmidt-Ott, A. (2006). Nanoparticle production using atmospheric pressure cold plasma. *Journal of Nanoparticle Research, 8*(5), 721–728. https://doi.org/10.1007/s11051-006-9133-2.

Voss, A., & Finlay, W. H. (2002). Deagglomeration of dry powder pharmaceutical aerosols. *International Journal of Pharmaceutics, 248*(1–2), 39–50. https://doi.org/10.1016/S0378-5173(02)00319-8.

Weber, A. P., & Friedlander, S. K. (1997). In situ determination of the activation energy for restructuring of nanometer aerosol agglomerates. *Journal of Aerosol Science, 28*(2), 179–192.